processes

MDPI

Article

Effect of Mn and Cu Substitution on the $SrFeO_3$ Perovskite for Potential Thermochemical Energy Storage Applications

Esraa Darwish, Moufida Mansouri, Duygu Yilmaz * and Henrik Leion

Chemistry and Chemical Engineering, Chalmers University of Technology, 41296 Gothenburg, Sweden; esraad@chalmers.se (E.D.); moufida@chalmers.se (M.M.); henrik.leion@chalmers.se (H.L.)
* Correspondence: duyguy@chalmers.se

Abstract: Perovskites are well-known oxides for thermochemical energy storage applications (TCES) since they show a great potential for spontaneous O_2 release due to their non-stoichiometry. Transition-metal-based perovskites are particularly promising candidates for TCES owing to their different oxidation states. It is important to test the thermal behavior of the perovskites for TCES applications; however, the amount of sample that can be used in thermal analyses is limited. The use of redox cycles in fluidized bed tests can offer a more realistic approach, since a larger amount of sample can be used to test the cyclic behavior of the perovskites. In this study, the oxygen release/consumption behavior of Mn- or Cu-substituted $SrFeO_3$ ($SrFe_{0.5}M_{0.5}O_3$; M: Mn or Cu) under redox cycling was investigated via thermal analysis and fluidized bed tests. The reaction enthalpies of the perovskites were also calculated via differential scanning calorimetry (DSC). Cu substitution in $SrFeO_3$ increased the performance significantly for both cyclic stability and oxygen release/uptake capacity. Mn substitution also increased the cyclic stability; however, the presence of Mn as a substitute for Fe did not improve the oxygen release/uptake performance of the perovskite.

Keywords: TCES; perovskite; redox

Citation: Darwish, E.; Mansouri, M.; Yilmaz, D.; Leion, H. Effect of Mn and Cu Substitution on the $SrFeO_3$ Perovskite for Potential Thermochemical Energy Storage Applications. *Processes* **2021**, *9*, 1817. https://doi.org/10.3390/pr9101817

Academic Editor: Ioannis Spanopoulos

Received: 26 August 2021
Accepted: 11 October 2021
Published: 13 October 2021

1. Introduction

The energy demand of the world is increasing day by day and the most commonly used energy sources are still fossil fuels [1,2]. Alternative energy sources have been sought, to overcome the adverse outcomes of the use of fossil fuels, such as global warming [3,4]. Renewable energy sources such as solar energy can be used for sustainable energy production [5]. However, combined energy storage systems should also be used to ensure the continuity of the supply where there is variation in energy production during the day [6]. Following the development of new energy storage methods such as thermochemical energy storage (TCES) systems, solar energy systems have received significant attention [7]. Thermochemical systems can store more energy than other thermal energy storage methods, since they involve a thermochemical reaction that requires a large amount of energy [8,9]. TCES systems require reversible chemical reactions, and due to the variety of available reactions they can work within a wide range of operational temperatures [8,10]. In a TCES process, the storage material undergoes chemical reactions that consist of charging and discharging stages [11]. In the charging stage, the heat is provided by solar power for the endothermic reaction, and the storage of heat is facilitated. In the discharging step, the stored energy is released via an exothermic reaction [8,12].

There are several materials that can exhibit the desired properties for thermochemical energy storage applications. These desired properties can be summarized as high reaction enthalpy, physical strength, and chemical resistance towards high operational temperatures [13,14]. In addition, candidate materials for TCES should be cost efficient, commercially available, non-toxic, and environmentally friendly [15,16]. From this point of view, metal oxides [17,18], mixed oxides [19–21], and perovskites [22–25] are attractive as TCES materials, since they can be used at high temperatures without the need

for product separation because a solid–gas reaction will take place during operation in these oxides [9,10,13,26]. The relevant chemical reactions should be reversible for TCES applications [27]. To obtain cyclic energy storage processes, the energy storage material should have the ability to release oxygen [28,29]. From this point of view, non-stoichiometric perovskite materials are very suitable for thermochemical energy storage applications [28,30,31].

Recently, $SrFeO_3$ has received great attention from researchers as a promising perovskite for thermochemical applications [32–37]. $SrFeO_3$ has been reported as a non-stoichiometric perovskite, with a stoichiometry depending on the temperature and the partial pressure of oxygen [38]. Although, $SrFeO_3$ itself is able to release/take up oxygen under appropriate conditions, a dopant addition can be useful for tuning the redox property of the perovskite [36]. A Mn dopant in $SrFeO_3$ has been reported to improve the cyclic stability of the perovskite [36]. A Cu addition has also been reported to increase the redox capacity of $SrFeO_3$ [36,39].

In this study, Cu and Mn were used for Fe substitution in $SrFeO_3$ ($SrFe_{0.5}M_{0.5}O_3$, M: Cu or Mn) perovskite, in order to investigate the effect on the cyclic stability of the perovskite in fluidized bed tests. The levels of the Cu and Mn substitutions were kept at 0.5 in the $SrFe_{0.5}M_{0.5}O_3$ system, to assess the effect of the equimolar combination of Cu–Fe and Mn–Fe in the Fe sites. Lower amounts of Cu and Mn additions have already been reported in the literature [36,39]; however, there are no studies using a fluidized bed reactor, which is closer to real applications than thermal analysis for investigating the cyclic stability performance of the perovskites.

2. Materials and Methods

The raw materials used in this study were $SrCO_3$ (Alfa Aesar™, >99.99%), Fe_2O_3 (Alfa Aesar™, >99.85%), CuO (Alfa Aesar™, >99.7%), and Mn_2O_3 (Alfa Aesar™, >98%) powders, and all of them were used as received. The perovskite samples were prepared via the solid-state synthesis method. The starting blends containing stoichiometric amounts of reactants for each perovskite were mixed in an agate mortar and pestle to obtain a homogeneous mixture. Ethanol was used as a dispersing agent to mix the powders thoroughly, and the mixing process was continued until the ethanol evaporated. The obtained mixtures were pressed into discs prior to the calcination step. The mixtures for $SrFeO_3$ and $SrFe_{0.5}Mn_{0.5}O_3$ were calcined at 700 °C for 5 h, and then the samples were ground in an agate mortar and pestle with ethanol. The calcination regime was 900 °C for 5 h for the $SrFe_{0.5}Cu_{0.5}O_3$ sample, and this sample was also ground after calcination. The calcined samples were heated in an oven, firstly at 1100 °C for 24 h and then at 1200 °C for 5 h. Heating and cooling rates were kept at 10 °C/min. The obtained samples were granulated via the wet granulation technique with the use of PVA as an organic binder. The binder-to-powder ratio was set to 0.005 by weight. Then, the powders were sieved to obtain the 125–180 µm size range.

Phase analyses of the synthesized samples were performed using an X-ray diffractometer (XRD, Bruker D8 Advance, Cu Kα, 40 kV, 40 mA) in the 2θ range of 20–60° with a step size of 0.01. A simultaneous thermal analyzer (Netzsch™-STA 409 PC Luxx) was used to reveal the thermal behavior of the samples by changing the temperature between 500 and 1000 °C during cycling. During the experiments, the STA was flushed with an air flow (pO_2: 0.21 atm) during the heating steps. During the cooling steps, the system was flushed with N_2 only. Several redox cycles consisting of consecutive heating and cooling steps were applied, to investigate the oxygen release/uptake behavior of the synthesized perovskites in a fluidized bed reactor.

A fluidized bed reactor with a length of 820 mm and a porous quartz plate of diameter 22 mm placed 370 mm from the bottom, were used to carry out the experiments. Five grams of sample was used in each experiment in the fluidized bed. The redox cycles were initiated by changing the temperature between 600 and 1050 °C in each cycle. During the oxidation cycles, the system was flushed with air (pO_2: 0.21 atm), and N_2 was used to

flush the reactor during the reduction cycles. The O_2 concentration in the outlet gas was detected using a Rosemount NGA 2000 multi-component gas analyzer.

3. Results and Discussion

The phase analyses of the $SrFeO_3$, $SrFe_{0.5}Mn_{0.5}O_3$ and $SrFe_{0.5}Cu_{0.5}O_3$ samples were carried out via XRD (Figure 1). $SrFeO_3$ was synthesized as a non-stoichiometric form of $SrFeO_3$, and the crystal structure of the perovskite was identified as cubic (PDF card #04-007-0078). $SrFe_{0.5}Cu_{0.5}O_3$ was also synthesized successfully, and it was identified as $SrFe_{0.75}Cu_{0.25}O_{2.1}$ (PDF card #04-023-6732) along with minor peaks related $Sr_3Fe_2O_{6.93}$ (PDF card #01-089-8241). The Cu-substituted $SrFeO_3$ was difficult to identify since there was no powder diffraction file belonging to $SrFe_{0.5}Cu_{0.5}O_3$ as a reference pattern in the database used. The formation of $Sr_3Fe_2O_{9.63}$ was most probably caused by some unreacted CuO during the heat treatment. However, no free CuO was observed in the XRD pattern; hence, it is assumed that $SrFe_{0.5}Cu_{0.5}O_3$ was formed. Similarly, the synthesis of $SrFe_{0.5}Mn_{0.5}O_3$ was successful as it could be identified via its characteristic peaks (PDF card #04-023-2570). The characterization studies necessary to obtain the exact compositions of the perovskites could not be carried out due to limitations and issues during the study. Therefore, it is worth noting that the samples were assumed to have the target composition as a result of the XRD analysis.

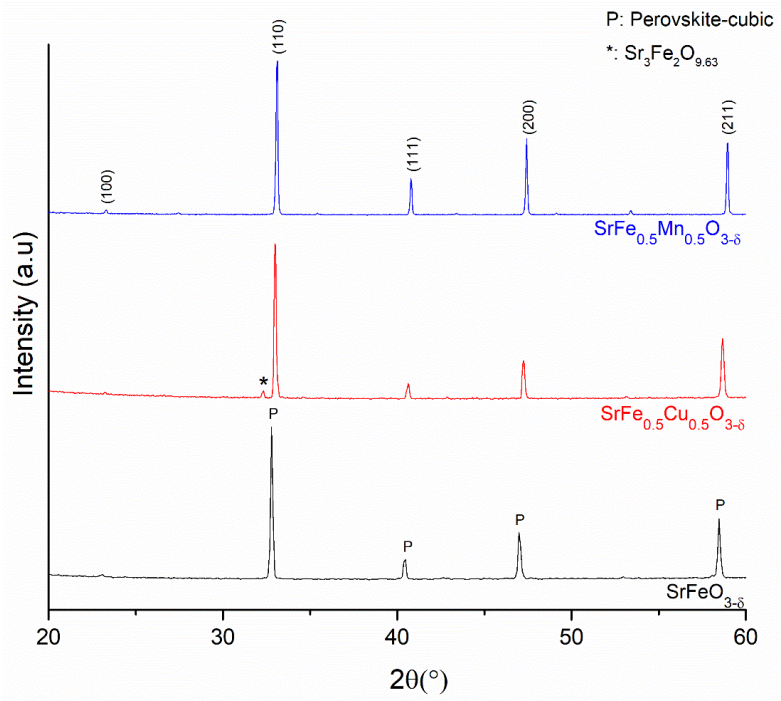

Figure 1. XRD patterns of the perovskites synthesized in the study.

The thermal analysis of the synthesized $SrFeO_3$ was carried out using a simultaneous thermal analyzer (Figure 2). $SrFeO_3$ showed sufficient cyclic stability in the STA analysis with respect to the mass loss/gain after four heating/cooling cycles. The average oxidation onset temperature was around 970 °C, while the average reduction onset temperature was around 530 °C. The average weight loss was 1.68 wt.% during the reduction steps, and the average weight gain was around 1.65 wt.% during the oxidation steps. The reaction enthalpy of $SrFeO_{3-\delta}$ oxidation was calculated as −118 kJ/mol O_2 from the relevant peak area of the DSC curve. The obtained enthalpy value was consistent with values from the literature [34,40].

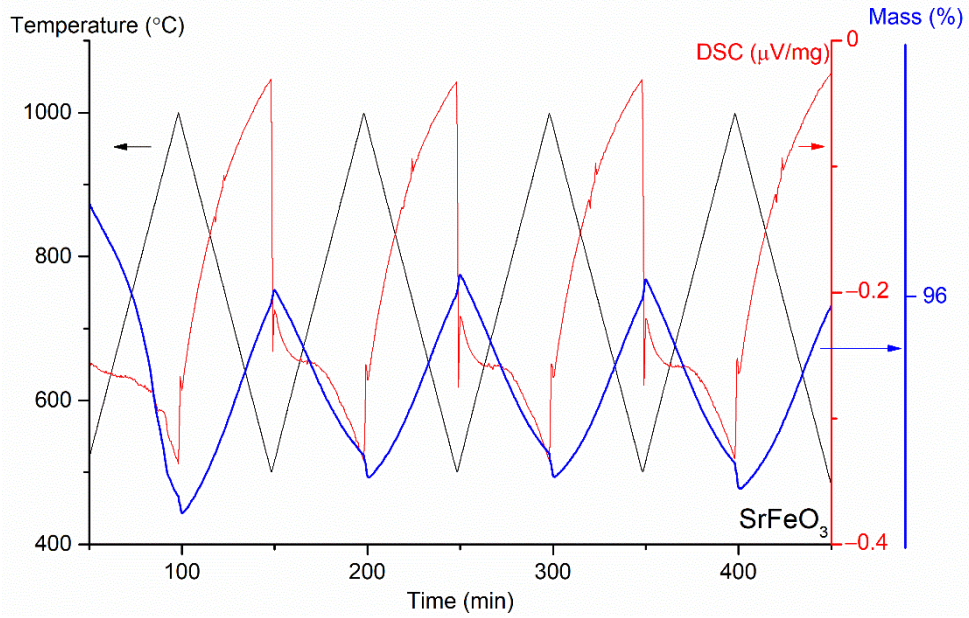

Figure 2. STA curves of the $SrFeO_3$ sample.

Thermal analysis is useful for revealing the thermal characteristics of materials with well-defined heating and cooling rates during cycling. However, the amount of material used in each experiment is limited. Nevertheless, the well-defined and precise heating/cooling rates do not represent the temperature profiles of real applications.

Fluidized bed tests are very useful for mimicking real applications for cyclic redox reactions. Since fluidized bed reactors have been reported as promising for use in TCES applications [41,42], the cyclic stability tests were carried out in a fluidized bed in this study. Figure 3 shows the O_2 release/uptake performance of the $SrFeO_3$ sample during the cyclic stability test in the fluidized bed. The fluidized bed test was designed with nine cycles for each sample, and each cycle took around 20 min from cooling to heating. The furnace of the fluidized bed setup was set to cycles consisting of heating to 1000 °C and cooling to 600 °C. In the fluidized bed test, the average reduction peak temperature was observed to be 755 °C, and the maximum O_2 peak during release was observed as 23.02 vol.%. The average oxidation peak temperature was around 950 °C, and the minimum O_2 in the system due to the O_2 uptake of the sample was detected as 20.54 vol.%. The cyclic stability of the material decreased marginally when the number of cycles increased. After the fifth cycle, the cycles appeared to have stabilized. There were no significant differences observed in the oxidation onset and the peak oxidation temperature in the thermal analysis and the fluidized bed tests. However, the reduction onset and the peak reduction temperatures varied significantly, both in the thermal analysis and the fluidized bed test. In the fluidized bed test, cooling was carried out down to 600 °C for operational reasons. This may be one of the reasons for the significantly different reduction temperatures. Although the onset and the peak temperatures are likely to differ anyway, it was expected that these temperatures would be only marginally different. However, it is known that the redox temperatures and the characteristics of $SrFeO_3$ are strongly dependent on the kinetic properties [38]. Therefore, different heating/cooling rates may be the reason for the varying reduction temperatures.

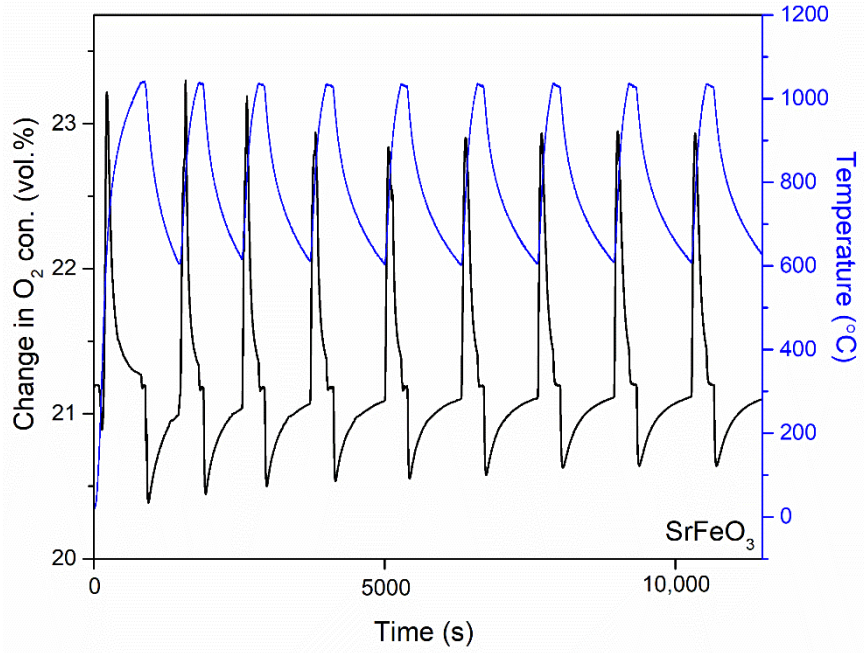

Figure 3. O_2 release/uptake performance of the $SrFe_{0.5}Mn_{0.5}O_3$ sample in the fluidized bed reactor.

To investigate the effect of Mn substitution in the $SrFeO_3$ system, both thermal analysis (Figure 4) and a fluidized bed test (Figure 5) were carried out. In the thermal analysis, the onset oxidation temperature was 970 °C, which was the same as for the pure $SrFeO_3$ system. However, the weight gain during oxidation was 0.84 wt.% which is only half that of the pure $SrFeO_3$. The onset reduction temperature was 520 °C in the thermal analysis, and an average of 0.73 wt.% weight loss was observed during the reduction steps. The onset reduction temperature of the $SrFe_{0.5}Mn_{0.5}O_3$ sample was the same as for the pure $SrFeO_3$. In the fluidized bed tests, the peak oxidation and the peak reduction temperatures were recorded as 958 °C and 794 °C, respectively. The redox peak temperature of the $SrFe_{0.5}Mn_{0.5}O_3$ sample was 40 °C higher than in the pure $SrFeO_3$. It is likely that Mn substitution increases the cyclic stability of the perovskite. The maximum O_2 release peak during the reduction (22.2 vol.%) and the O_2 uptake (20.45 vol.%) during the oxidation, decreased when the $SrFe_{0.5}Mn_{0.5}O_3$ sample was tested in the fluidized bed. Even though Mn substitution did not increase the O_2 release/uptake capacity of the $SrFeO_3$ system, the cyclic stability of the perovskite improved with Mn substitution, particularly in the fluidized bed tests. In addition to this, the reaction enthalpy of the system also increased compared to $SrFeO_3$; it was calculated as −432 kJ/mol O_2 for the system with Mn substitution. The higher oxidation enthalpy of $SrMnO_3$ compared to $SrFeO_3$ was previously reported [36]. Hence, the higher enthalpy of Mn-substituted $SrFeO_3$ compared with pure $SrFeO_3$ obtained in this study was consistent with the literature.

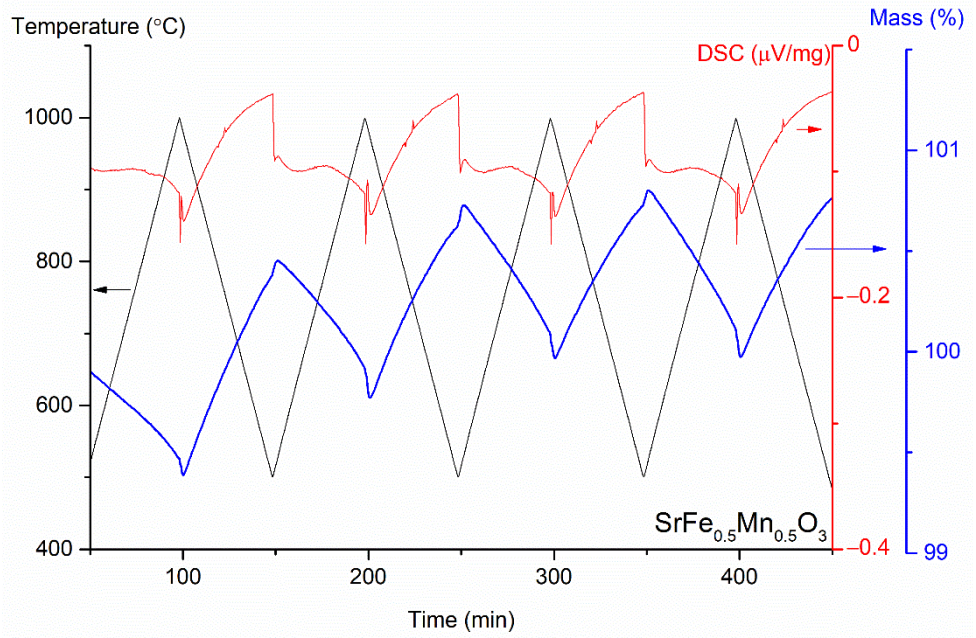

Figure 4. STA curves of the $SrFe_{0.5}Mn_{0.5}O_3$ sample.

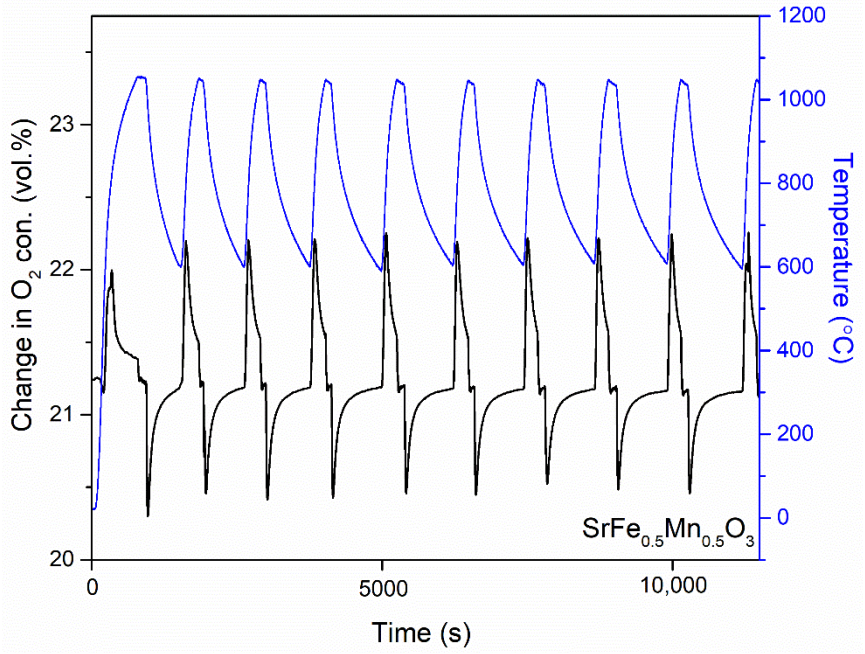

Figure 5. O_2 release/uptake performance of the $SrFe_{0.5}Mn_{0.5}O_3$ sample in the fluidized bed reactor.

The efficiency of the perovskite was significantly improved when Cu was substituted into the $SrFeO_3$ system. The average weight loss was calculated as 1.59 wt.% during the reduction, and the onset reduction temperature was 520 °C (Figure 6). The onset oxidation temperature was around 960 °C, and the average weight gain was calculated as 1.74 wt.%. The reaction enthalpy was calculated as −209 kJ/mol O_2 for the $SrFe_{0.5}Cu_{0.5}O_3$ sample. These results show that Cu substitution reduced the redox onset temperatures by around 10 °C. The weight changes of the $SrFe_{0.5}Cu_{0.5}O_3$ sample in the thermal analysis were slightly higher than those of the $SrFeO_3$ sample, and twice as high as those of the $SrFe_{0.5}Mn_{0.5}O_3$ sample. In the fluidized bed tests, the redox peak temperature was 758 °C, and the maximum O_2 release peak during the reduction steps was 23.11 vol.% (Figure 7). Although the $SrFe_{0.5}Cu_{0.5}O_3$ sample had a similar reduction peak temperature to that of the $SrFeO_3$ sample, the amount of O_2 released during the reduction was increased. This result

was not surprising, since Cu doping of $SrFeO_3$ has been reported to improve the oxygen storage capacity [39]. The oxidation peak temperature was 893 °C for the $SrFe_{0.5}Cu_{0.5}O_3$ sample, which was around 60 °C lower than for the pure and Mn-substituted $SrFeO_3$. This is probably due to the different oxygen affinities of the related metals [36]. During oxidation, the O_2 concentration in the fluidized bed decreased on average by 20.62 vol.%.

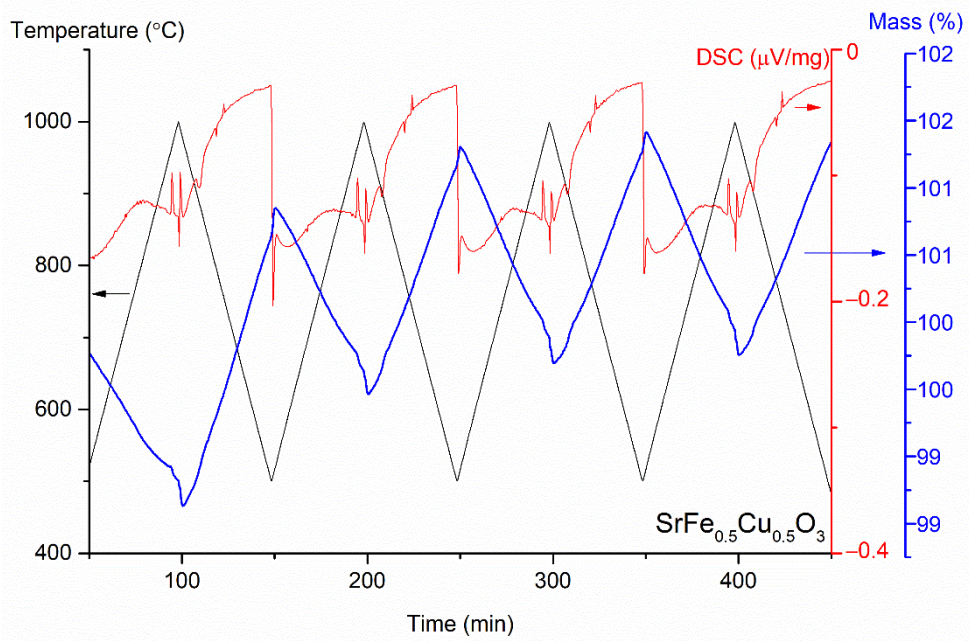

Figure 6. STA curves of the $SrFe_{0.5}Cu_{0.5}O_3$ sample.

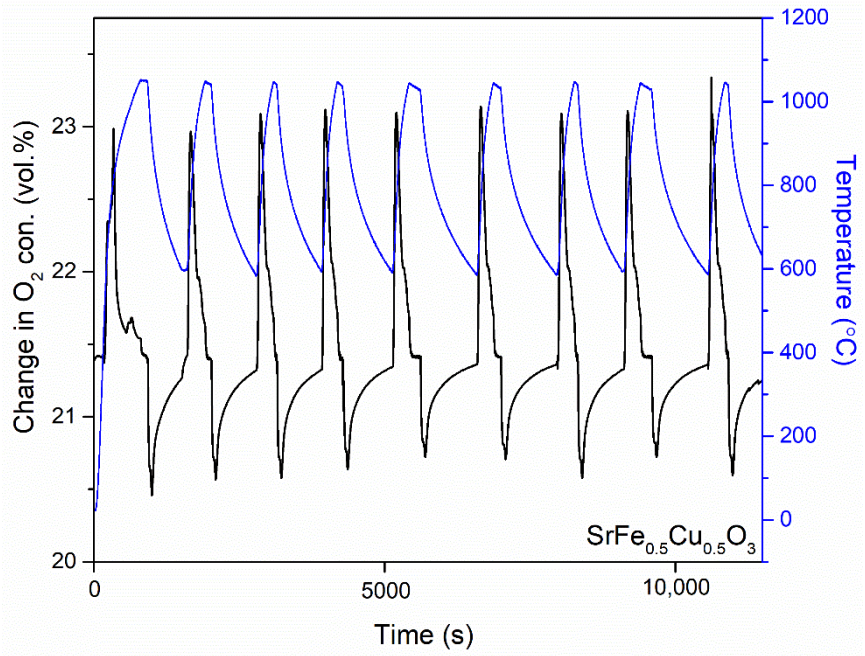

Figure 7. STA curves of the $SrFe_{0.5}Cu_{0.5}O_3$ sample.

It should be noted that the first cycles of the STA analyses were not taken into consideration in this study, since it is known that the first cycles are particularly affected by drift. The reaction enthalpies that were calculated via the STA analyses were assumed to consist of the heat associated with the formation of oxygen vacancies, the heat associated with the phase transition, and the sensible heat, although a detailed investigation could not be carried out due to technical limitations.

The oxygen non-stoichiometry values (δ) of the samples, as shown in Figure 8, were calculated using Equation (1) [43]. The molecular weight and the sample weight were denoted by M and w, respectively, w_p is the sample weight at 950 °C under reducing conditions where the δ value is assumed to be the lowest obtained experimentally, and w_x is the sample weight at a given temperature.

$$\delta = \frac{w_x - w_p}{M_{O_2}} \times \frac{M_p}{w_p} \quad (1)$$

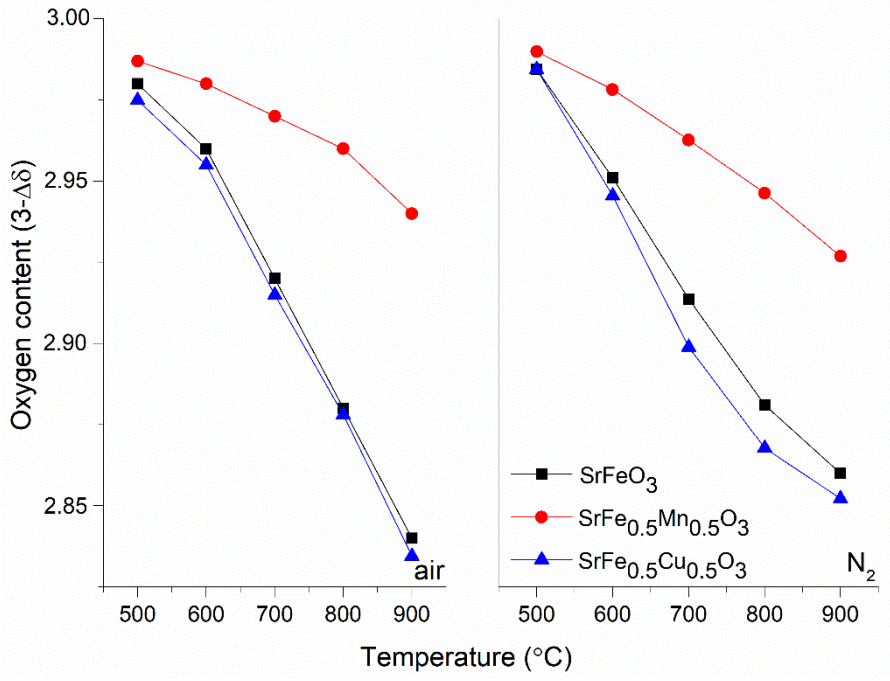

Figure 8. Oxygen content of the samples in this study during reduction and oxidation as a function of temperature, obtained via STA.

During heating and cooling in the STA, the system was flushed with air (pO_2: 0.21 atm) and nitrogen, respectively, and the weight changes were recorded during the temperature change. The maximum oxygen non-stoichiometry (δ) (corresponding to the minimum oxygen content in the samples) was observed for the $SrFe_{0.5}Cu_{0.5}O_3$ sample. The minimum δ values were observed for $SrFe_{0.5}Mn_{0.5}O_3$, which is consistent with the fluidized bed tests. These results show that Cu substitution in the $SrFeO_3$ sample improved the O_2 release/uptake ability of the perovskite. The oxygen content of the $SrFeO_3$ sample in this study had lower oxygen vacancy (δ) values compared to related studies in the literature [43]. This is probably due to the different heating/cooling rates applied during the redox experiments. The initial $SrFeO_3$ sample was assumed to be fully oxidized before the experiments started. In the literature, it was reported that Cu and Mn dopants in the $SrFeO_3$ system improved the oxygen capacity [36], and higher oxygen capacities were obtained for both Cu- and Mn-substituted $SrFeO_3$. However, the level of substitution was in that case far lower than in this study. Therefore, a lower level of Cu or Mn substitution can be recommended to improve the oxygen capacity of the pure $SrFeO_3$.

4. Conclusions

In this study, Cu and Mn substitutions in the $SrFeO_3$ perovskite system were tested for potential thermochemical energy storage applications. The cyclic stability of the perovskite was tested in a fluidized bed reactor, and the thermal behavior was analyzed using a thermal analyzer. Both Cu and Mn substitution increased the oxidation reaction enthalpy of the pure $SrFeO_3$. However, the highest oxidation enthalpy was obtained for the Mn-

substituted $SrFeO_3$ system. Both substitutions improved the cyclic stability of the pure $SrFeO_3$ in the fluidized bed tests, but $SrFe_{0.5}Mn_{0.5}O_3$ showed a lower performance with respect to O_2 release/uptake.

Author Contributions: Conceptualization, D.Y. and H.L.; methodology, E.D. and M.M.; validation, D.Y. and M.M; investigation, E.D.; resources, H.L.; writing—original draft preparation, E.D.; writing—review and editing, D.Y. and H.L.; visualization, E.D.; supervision, D.Y. and H.L.; project administration, D.Y. and H.L.; funding acquisition, D.Y. and H.L. All authors have read and agreed to the published version of the manuscript.

Funding: This project was funded by the Adlerbertska Foundation (21285157) and Iris Stipendiet (IR2020-0195).

Conflicts of Interest: The authors declare no conflict of interest.

References

1. Amirante, R.; Cassone, E.; Distaso, E.; Tamburrano, P. Overview on recent developments in energy storage: Mechanical, electrochemical and hydrogen technologies. *Energy Convers. Manag.* **2017**, *132*, 372–387. [CrossRef]
2. Wilson, I.A.G.; Styring, P. Why Synthetic Fuels Are Necessary in Future Energy Systems. *Front. Energy Res.* **2017**, *5*, 1–10. [CrossRef]
3. Gielen, D.; Boshell, F.; Saygin, D.; Bazilian, M.D.; Wagner, N.; Gorini, R. The role of renewable energy in the global energy transformation. *Energy Strateg. Rev.* **2019**, *24*, 38–50. [CrossRef]
4. Zou, C.; Zhao, Q.; Zhang, G.; Xiong, B. Energy revolution: From a fossil energy era to a new energy era. *Nat. Gas Ind. B* **2016**, *3*, 1–11. [CrossRef]
5. Kuravi, S.; Trahan, J.; Goswami, D.Y.; Rahman, M.M.; Stefanakos, E.K. Thermal energy storage technologies and systems for concentrating solar power plants. *Prog. Energy Combust. Sci.* **2013**, *39*, 285–319. [CrossRef]
6. Evans, A.; Strezov, V.; Evans, T.J. Assessment of utility energy storage options for increased renewable energy penetration. *Renew. Sustain. Energy Rev.* **2012**, *16*, 4141–4147. [CrossRef]
7. Cabeza, L.F.; Martorell, I.; Miró, L.; Fernández, A.I.; Barreneche, C. *Introduction to Thermal Energy Storage (TES) Systems*; Woodhead Publishing Limited: Sawston, UK, 2015.
8. Pardo, P.; Deydier, A.; Anxionnaz-Minvielle, Z.; Rougé, S.; Cabassud, M.; Cognet, P. A review on high temperature thermochemical heat energy storage. *Renew. Sustain. Energy Rev.* **2014**, *32*, 591–610. [CrossRef]
9. Solé, A.; Martorell, I.; Cabeza, L.F. State of the art on gas-solid thermochemical energy storage systems and reactors for building applications. *Renew. Sustain. Energy Rev.* **2015**, *47*, 386–398. [CrossRef]
10. Prieto, C.; Cooper, P.; Fernández, A.I.; Cabeza, L.F. Review of technology: Thermochemical energy storage for concentrated solar power plants. *Renew. Sustain. Energy Rev.* **2016**, *60*, 909–929. [CrossRef]
11. Stutz, B.; Le Pierrès, N.; Kuznik, F.; Johannes, K.; Del Barrio, E.P.; Bédécarrats, J.-P.; Gibout, S.; Marty, P.; Zalewski, L.; Soto, J.; et al. Storage of thermal solar energy. *Comptes Rendus Phys.* **2017**, *18*, 401–414. [CrossRef]
12. Abedin, A.H.; Rosen, M.A. Assessment of a closed thermochemical energy storage using energy and exergy methods. *Appl. Energy* **2012**, *93*, 18–23. [CrossRef]
13. André, L.; Abanades, S.; Flamant, G. Screening of thermochemical systems based on solid-gas reversible reactions for high temperature solar thermal energy storage. *Renew. Sustain. Energy Rev.* **2016**, *64*, 703–715. [CrossRef]
14. Wu, S.; Zhou, C.; Doroodchi, E.; Nellore, R.; Moghtaderi, B. A review on high-temperature thermochemical energy storage based on metal oxides redox cycle. *Energy Convers. Manag.* **2018**, *168*, 421–453. [CrossRef]
15. Gil, A.; Medrano, M.; Martorell, I.; Lázaro, A.; Dolado, P.; Zalba, B.; Cabeza, L.F. State of the art on high temperature thermal energy storage for power generation. Part 1-Concepts, materials and modellization. *Renew. Sustain. Energy Rev.* **2010**, *14*, 31–55. [CrossRef]
16. Zalba, L.F.; Marın, J.M.; Cabeza, L.F.; Mehling, H. Review on Phase changing materials to store energy. *Appl. Therm. Eng.* **2003**, *23*, 251–283. [CrossRef]
17. Carrillo, A.J.; Serrano, D.P.; Pizarro, P.; Coronado, J.M. Thermochemical heat storage based on the Mn2O3/Mn3O4 redox couple: Influence of the initial particle size on the morphological evolution and cyclability. *J. Mater. Chem. A* **2014**, *2*, 19435–19443. [CrossRef]
18. Carrillo, A.J.; Sastre, D.; Serrano, D.P.; Pizarro, P.; Coronado, J.M. Revisiting the BaO2/BaO redox cycle for solar thermochemical energy storage. *Phys. Chem. Chem. Phys.* **2016**, *18*, 8039–8048. [CrossRef]
19. Carrillo, A.J.; Serrano, D.P.; Pizarro, P.; Coronado, J.M. Understanding Redox Kinetics of Iron-Doped Manganese Oxides for High Temperature Thermochemical Energy Storage. *J. Phys. Chem. C* **2016**, *120*, 27800–27812. [CrossRef]
20. Carrillo, A.J.; Moya, J.; Bayón, A.; Jana, P.; O'Shea, V.A.D.L.P.; Romero, M.; Gonzalez-Aguilar, J.; Serrano, D.; Pizarro, P.; Coronado, J.M. Thermochemical energy storage at high temperature via redox cycles of Mn and Co oxides: Pure oxides versus mixed ones. *Sol. Energy Mater. Sol. Cells* **2014**, *123*, 47–57. [CrossRef]

21. Buck, R.; Agrafiotis, C.; Tescari, S.; Neumann, N.; Schmücker, M. Techno-Economic Analysis of Candidate Oxide Materials for Thermochemical Storage in Concentrating Solar Power Systems. *Front. Energy Res.* **2021**, *9*, 1–13. [CrossRef]
22. Mastronardo, E.; Qian, X.; Coronado, J.M.; Haile, S. Fe-doped CaMnO3 for thermochemical heat storage application. *AIP Conf. Proc.* **2019**, *2126*, 210005.
23. Imponenti, L.; Albrecht, K.J.; Kharait, R.; Sanders, M.D.; Jackson, G.S. Redox cycles with doped calcium manganites for thermochemical energy storage to 1000 °C. *Appl. Energy* **2018**, *230*, 1–18. [CrossRef]
24. Babiniec, S.M.; Coker, E.N.; Ambrosini, A.; Miller, J.E. ABO3 (A = La, Ba, Sr, K.; B = Co, Mn, Fe) perovskites for thermochemical energy storage. *AIP Conf. Proc.* **2016**, *1734*, 050006.
25. Babiniec, S.M.; Coker, E.N.; Miller, J.E.; Ambrosini, A. Investigation of $La_xSr_{1-x}Co_yM_{1-y}O_{3-\delta}$ (M=Mn, Fe) perovskite materials as thermochemical energy storage media. *Sol. Energy* **2015**, *118*, 451–459. [CrossRef]
26. Ströhle, S.; Haselbacher, A.; Jovanovic, Z.R.; Steinfeld, A. The effect of the gas-solid contacting pattern in a high-temperature thermochemical energy storage on the performance of a concentrated solar power plant. *Energy Environ. Sci.* **2016**, *9*, 1375–1389. [CrossRef]
27. Tescari, S.; Agrafiotis, C.; Breuer, S.; de Oliveira, L.; Puttkamer, M.N.-V.; Roeb, M.; Sattler, C. Thermochemical solar energy storage via redox oxides: Materials and reactor/heat exchanger concepts. *Energy Procedia* **2013**, *49*, 1034–1043. [CrossRef]
28. André, L.; Abanades, S. Recent Advances in Thermochemical Energy Storage via Solid–Gas Reversible Reactions at High Temperature. *Energies* **2020**, *13*, 5859. [CrossRef]
29. Yilmaz, D.; Darwish, E.; Leion, H. Investigation of the combined Mn-Si oxide system for thermochemical energy storage applications. *J. Energy Storage* **2020**, *28*, 101180. [CrossRef]
30. Mastronardo, E.; Qian, X.; Coronado, J.M.; Haile, S.M. Impact of La doping on the thermochemical heat storage properties of CaMnO3-δ. *J. Energy Storage* **2021**, *40*, 102793. [CrossRef]
31. Jin, F.; Xu, C.; Yu, H.; Xia, X.; Ye, F.; Li, X.; Du, X.; Yang, Y. CaCo0.05Mn0.95O3-δ: A Promising Perovskite Solid Solution for Solar Thermochemical Energy Storage. *ACS Appl. Mater. Interfaces* **2021**, *13*, 3856–3866. [CrossRef] [PubMed]
32. Zhang, Z.; Andre, L.; Abanades, S. Experimental assessment of oxygen exchange capacity and thermochemical redox cycle behavior of Ba and Sr series perovskites for solar energy storage. *Sol. Energy* **2016**, *134*, 494–502. [CrossRef]
33. Farr, T.P.; Nguyen, N.P.; Bush, H.E.; Ambrosini, A.; Loutzenhiser, P.G. Perovskites for Solar Thermochemical Air Separation. *Materials* **2020**, *13*, 5123. [CrossRef]
34. Haavik, C.; Atake, T.; Stølen, S. On the enthalpic contribution to the redox energetics of $SrFeO_{3-\delta}$. *Phys. Chem. Chem. Phys.* **2002**, *4*, 1082–1087. [CrossRef]
35. Haavik, C.; Atake, T.; Kawaji, H.; Stølen, S. On the entropic contribution to the redox energetics of $SrFeO_{3-\delta}$. *Phys. Chem. Chem. Phys.* **2001**, *3*, 3863–3870. [CrossRef]
36. Krzystowczyk, E.; Wang, X.; Dou, J.; Haribal, V.; Li, F. Substituted $SrFeO_3$ as robust oxygen sorbents for thermochemical air separation: Correlating redox performance with compositional and structural properties. *Phys. Chem. Chem. Phys.* **2020**, *22*, 8924–8932. [CrossRef]
37. Takeda, Y.; Kanno, K.; Takada, T.; Yamamoto, O.; Takano, M.; Nakayama, N.; Bando, Y. Phase relation in the oxygen nonstoichiometric system, $SrFeO_x$ ($2.5 \leq x \leq 3.0$). *J. Solid State Chem.* **1986**, *63*, 237–249. [CrossRef]
38. Bulfin, B.; Vieten, J.; Naik, J.M.; Ricarda, P.G.; Roeb, M.; Sattler, C.; Steinfeld, A. Isothermal relaxation kinetics for the reduction and oxidation of $SrFeO_3$ based perovskites. *Phys. Chem. Chem. Phys.* **2020**, *22*, 2466–2474. [CrossRef]
39. Vieten, J.; Bulfin, B.; Starr, D.E.; Hariki, A.; de Groot, F.M.; Azarpira, A.; Zachäus, C.; Hävecker, M.; Skorupska, K.; Knoblauch, N.; et al. Redox Behavior of Solid Solutions in the $SrFe_{1-x}Cu_xO_{3-\delta}$ System for Application in Thermochemical Oxygen Storage and Air Separation. *Energy Technol.* **2019**, *7*, 131–139. [CrossRef]
40. Vieten, J.; Bulfin, B.; Senholdt, M.; Roeb, M.; Sattler, C.; Schmücker, M. Redox thermodynamics and phase composition in the system $SrFeO_{3-\delta}$—$SrMnO_{3-\delta}$. *Solid State Ionics* **2017**, *308*, 149–155. [CrossRef]
41. Wong, B. *Thermochemical Heat Storage for Concentrated Solar Power*; Final Report for the US Depaartment Energy: San Diego, CA, USA, 30 April 2011.
42. Tregambi, C.; Montagnaro, F.; Salatino, P.; Solimene, R. Directly irradiated fluidized bed reactors for thermochemical processing and energy storage: Application to calcium looping. *AIP Conf. Proc.* **2017**, *1850*, 090007.
43. Ikeda, H.; Nikata, S.; Hirakawa, E.; Tsuchida, A.; Miura, N. Oxygen sorption/desorption behavior and crystal structural change for $SrFeO_{3-\delta}$. *Chem. Eng. Sci.* **2016**, *147*, 166–172. [CrossRef]